iScience

CellPress
OPEN ACCESS

Article

Highly sensitive visual restoration and protection via ectopic expression of chimeric rhodopsin in mice

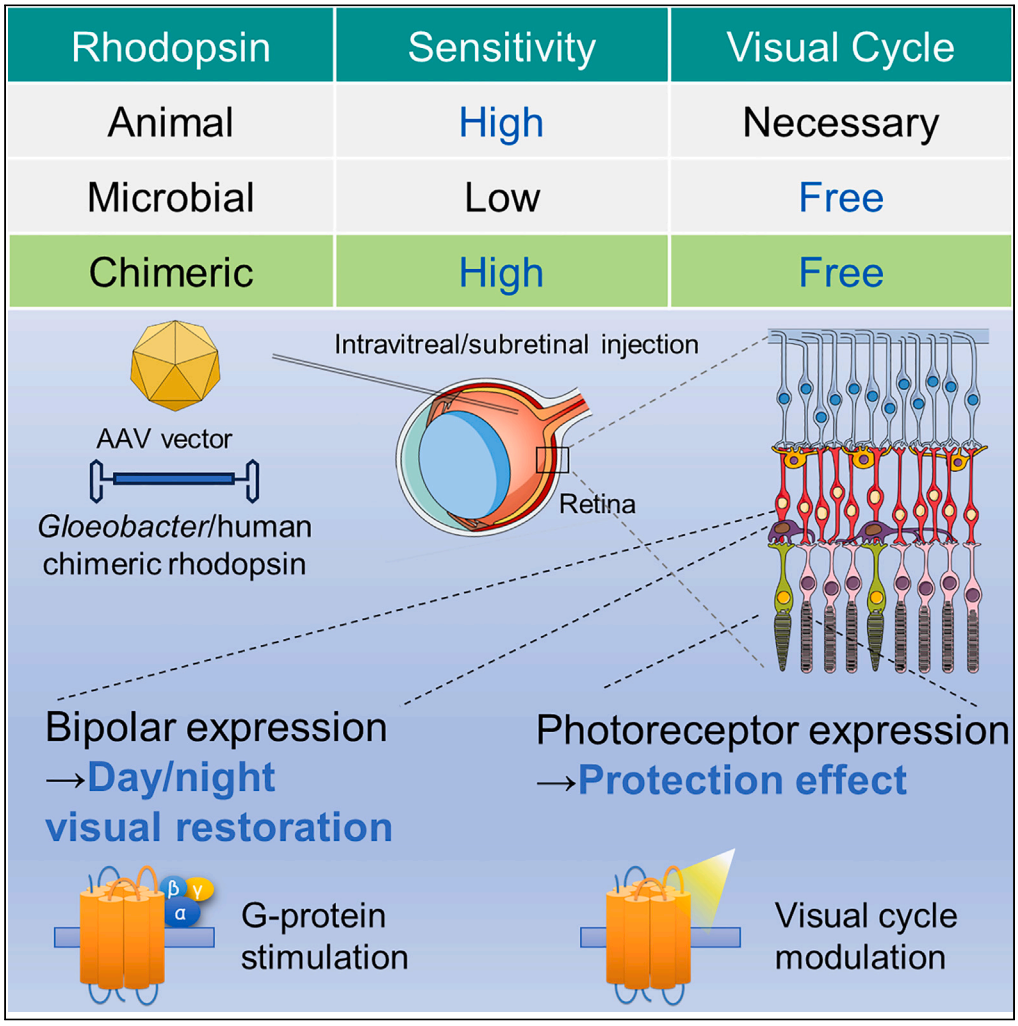

Yusaku Katada, Kazuho Yoshida, Naho Serizawa, ..., Hideki Kandori, Kazuo Tsubota, Toshihide Kurihara

kurihara@z8.keio.jp

Highlights

Hybrid animal and microbial rhodopsin achieves high sensitivity without a visual cycle

Bipolar expression of GHCR achieves day/night visual restoration

Photoreceptor expression of GHCR achieves protection against retinal degeneration

Katada et al., iScience 26, 107716
October 20, 2023
https://doi.org/10.1016/j.isci.2023.107716

iScience

CellPress
OPEN ACCESS

Article

Highly sensitive visual restoration and protection via ectopic expression of chimeric rhodopsin in mice

Yusaku Katada,[1,2] Kazuho Yoshida,[3] Naho Serizawa,[1,2,4] Deokho Lee,[1,2] Kenta Kobayashi,[5] Kazuno Negishi,[2] Hideyuki Okano,[6] Hideki Kandori,[3] Kazuo Tsubota,[7] and Toshihide Kurihara[1,2,8,*]

SUMMARY

Photoreception requires amplification by mammalian rhodopsin through G protein activation, which requires a visual cycle. To achieve this in retinal gene therapy, we incorporated human rhodopsin cytoplasmic loops into *Gloeobacter* rhodopsin, thereby generating *Gloeobacter* and human chimeric rhodopsin (GHCR). In a murine model of inherited retinal degeneration, we induced retinal GHCR expression by intravitreal injection of a recombinant adeno-associated virus vector. Retinal explant and visual thalamus electrophysiological recordings, behavioral tests, and histological analysis showed that GHCR restored dim-environment vision and prevented the progression of retinal degeneration. Thus, GHCR may be a potent clinical tool for the treatment of retinal disorders.

INTRODUCTION

Inherited retinal degeneration (IRD) is a major cause of vision loss. More than 2 million people worldwide are blind due to IRD,[1] and few effective treatments exist. For retinitis pigmentosa (RP), one of the most common forms of IRD, previous studies have reported vision restoration in animal models using various molecules as optogenetic actuators.[2–9] In addition, clinical trials are under way to investigate the effects of introducing channelrhodopsin 2 (RST-001, ClinicalTrials.gov Identifier: NCT01648452) and ChrimsonR (GS-030, ClinicalTrials.gov Identifier: NCT03326336) into retinal ganglion cells (RGCs) via gene transduction achieved by intravitreal injection of recombinant adeno-associated virus (rAAV). The first clinical case report on optogenetic therapy was recently reported.[10] However, microbial opsins, such as channelrhodopsin 2, require high light intensity, such as outdoor light intensity levels, to function.[11–13] They cannot restore vision in dimly lit environments, such as indoors or at night, and strong light irradiation can promote retinal degeneration.[14,15] Physiological photoreception mediated by mammalian rhodopsin, however, relies on amplification through G protein activation. Although the introduction of vertebrate opsin improved photosensitivity in mice,[9,16] it is unclear how the chromophore retinal is metabolized in the retina where the visual cycle is broken. Animal rhodopsin also causes toxicity if all-trans retinal is not properly metabolized,[17,18] and is, thus, hampered by safety and stability concerns in terms of clinical application.

Because of the previous limitations of animal visual opsins, one attempt to circumvent them is the chimeric rhodopsin of melanopsin and G protein-coupled receptor (GPCR).[8,19] Melanopsin is a non-visual opsin, and despite being an animal opsin, it is not easily photobleached. However, it has a "bistable" photo-cycle and requires different wavelengths of light for conformational change, which may result in unnatural appearance.[20,21]

Therefore, a chimeric rhodopsin of microbial opsin and GPCR,[22–24] is not photo-bleached and is a monostable pigment like visual opsin, but may be able to achieve highly sensitive visual restoration via G protein stimulation.

In this study, to achieve light sensitivity, stability, and safety, we attempted to restore vision in mice using *Gloeobacter* and human chimeric rhodopsin (GHCR).[23,24]

[1]Laboratory of Photobiology, Keio University School of Medicine, Shinjuku-ku, Tokyo 160-8582, Japan
[2]Department of Ophthalmology, Keio University School of Medicine, Shinjuku-ku, Tokyo 160-8582, Japan
[3]Department of Life Science and Applied Chemistry, Nagoya Institute of Technology, Nagoya, Aichi 466-0061, Japan
[4]Department of Nutritional Sciences, Toyo University, Kita-ku, Tokyo 115-8650, Japan
[5]Section of Viral Vector Development, Center for Genetic Analysis of Behavior, National Institute for Physiological Sciences, National Institutes of Natural Sciences, Okazaki, Aichi 444-8585, Japan
[6]Department of Physiology, Keio University School of Medicine, Shinjuku-ku, Tokyo 160-8582, Japan
[7]Tsubota Laboratory, Inc., Shinjuku-ku, Tokyo 160-0016, Japan
[8]Lead contact
*Correspondence: kurihara@z8.keio.jp
https://doi.org/10.1016/j.isci.2023.107716

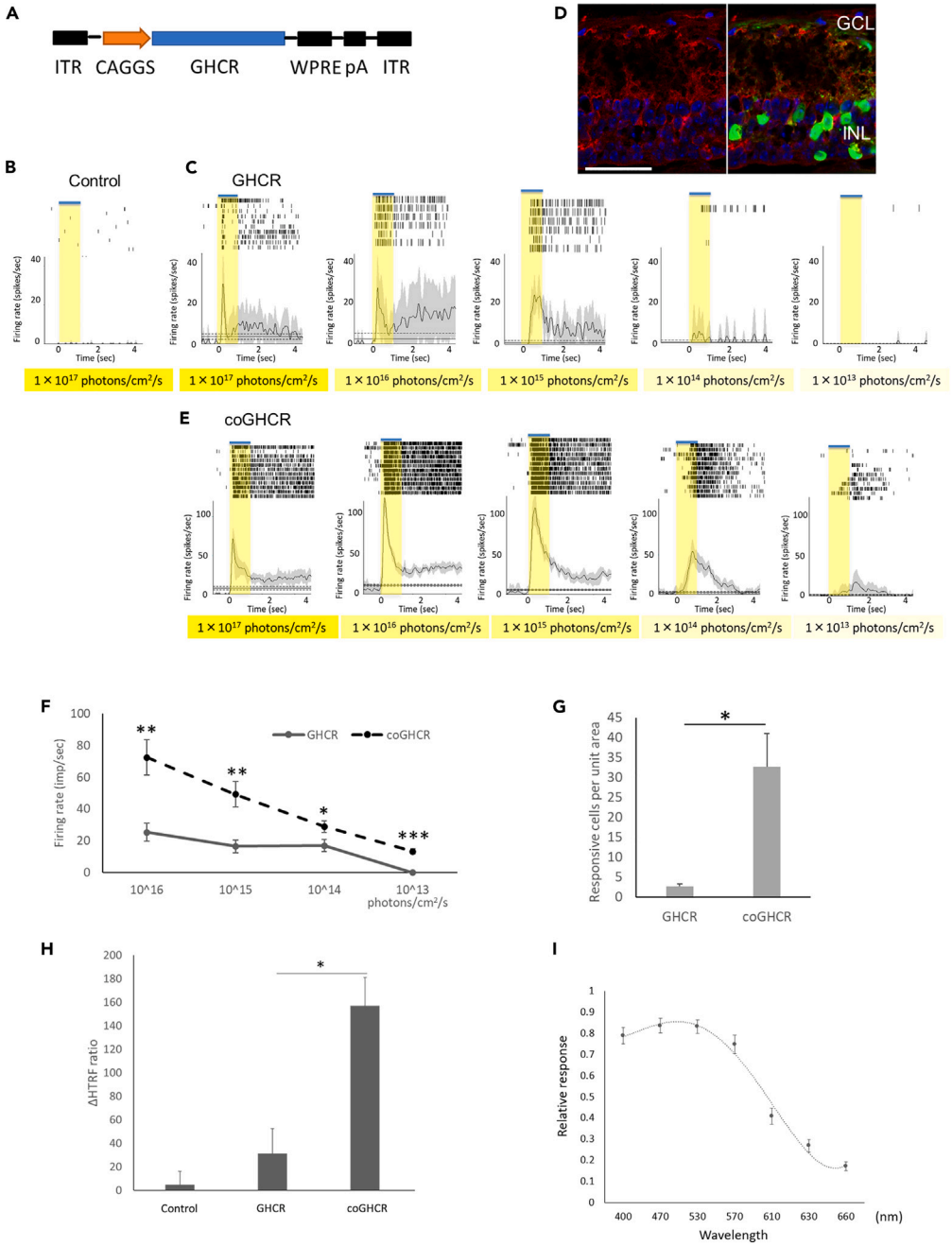

Figure 1. Ectopic GHCR expression restores light responses in the *rd1* mouse retina

(A) DNA expression cassette schematic. The GHCR coding sequence is driven by the CAGGS promoter, flanked by inverted terminal repeats (ITR), and stabilized by a polyadenylation signal sequence (pA) and a woodchuck hepatitis posttranscriptional regulatory element (WPRE).

(B, C, and E) Raster plots and peri-stimulus time histograms for light stimulation of control (AAV-DJ-CAGGS-EGFP) (B), GHCR-treated (AAV-DJ-CAGGS-GHCR) (C), and coGHCR-treated (AAV-DJ-CAGGS-coGHCR) mice (E). Responses to exposure to a white LED with varying light intensity for 1.0 s. Gray shading around the averaged traces represents the standard error of the mean (SEM).

(D) Confocal image of a transverse *rd1* mouse retina section 2 months after AAV-DJ-CAGGS-coGHCR intravitreal injection. Green, FLAG tag antibody signal (vector); red, PKCα signal (bipolar cells); blue, 4′,6-diamidino-2-phenylindolenuclear (DAPI) counterstaining. Scale bar, 50 μm.

(F) Quantitation of the firing rates of RGCs transduced with GHCR or coGHCR at the indicated light intensity.

(G) Histogram showing the number of RGCs that responded to light per unit area (2.6 mm^2) of the retinas of GHCR- or coGHCR-treated mice (n = 3 each).

(H) Changes in cAMP consumption in response to Gi/o-coupled G-protein-coupled receptor activation in HEK293T cells transfected with GHCR and coGHCR (n = 3 each).

Figure 1. *Continued*

(I) Spectral sensitivity induced by coGHCR (n = 23 cells each). Error bars represent the SEM. Data were analyzed with Student's two-tailed t-test in (F and G) and one-way analysis of variance (ANOVA) and Tukey's multiple comparison test in (H); * represents $p \leq 0.05$, ** represents $p \leq 0.01$, and *** represents $p \leq 0.001$. GHCR, *Gloeobacter* and human chimeric rhodopsin; coGHCR, codon-optimized *Gloeobacter* and human chimeric rhodopsin; GCL, ganglion cell layer; INL, inner nuclear layer.

RESULTS

Design of GHCR

Although there is no sequence identity between microbial and animal opsin, both possess similar chromophore (retinal) and protein (seven-transmembrane helix) structures. As we previously reported,[24] to generate GHCR, we replaced the second and third intracellular loops of *Gloeobacter* rhodopsin with human sequences and introduced the E132Q mutation (Figure S1). Previous work has shown that GHCR induces G protein activation *in vitro*.[24]

Restoring light-evoked activity in the retina with GHCR

We injected a viral vector (rAAV-DJ or rAAV-2) containing the GHCR coding sequence under the control of the hybrid promoter comprising the CMV immediate-early enhancer, CBA promoter, and CBA intron 1/exon 1, known as the CAGGS promoter, (CAGGS-GHCR; Figure 1A) into the vitreous humor of 10-week-old *rd1* mice. We adopted the rAAV-DJ vector to achieve more efficient, widespread gene transfer,[25,26] and used rAAV-2 as a benchmark, as it has already been used in the clinic.[27] The retinas were harvested 2–4 months later. Enhanced green fluorescent protein (EGFP) reporter gene expression was observed in both the ganglion cell layer and the inner nuclear layer (Figures S2A and S2B). To evaluate the function of ectopically expressed GHCR in the mouse retina, we performed multi-electrode array (MEA) recording to record the extracellular potential of RGCs. As a result of photoreceptor degeneration, the untreated control retina showed no RGC response as detected by MEA (Figure 1B). In contrast, the treated retinas showed obvious light-induced responses down to 10^{14} photons/cm^2/s of white light-emitting diode (LED) irradiation (Figure 1C).

Next, to create a stable vector for human gene therapy, we designed a codon-optimized version of GHCR (coGHCR) and fused the ER2 endoplasmic reticulum (ER) export signal to its C-terminus to increase gene expression levels. Immunolabeling revealed expression across the whole retina, including in the bipolar cells, of treated *rd1* mice (Figure 1D). As a result, the firing rate increased significantly, and a photoresponse was confirmed down to 10^{13} photons/cm^2/s, which had not observed before optimization (Figures 1E, 1F, and S2C). The retinas of WT mice were highly responsive to all light stimulus levels under dark-adapted conditions, but under light-adapted conditions, the firing rate was also modulated in response to light stimulus intensity, and coGHCR response was similar to the light-adapted conditions in WT mice (Figure S2D). No photoresponse to any light stimulus level was obtained from control untreated mice. Moreover, the number of firing cells per unit area also increased significantly (Figure 1G). Since rhodopsin shows selectivity for Gi/o class G proteins upon heterologous expression,[28–31] we measured Gi/o activation with a homogeneous time-resolved fluorescence (HTRF) cyclic adenosine monophosphate (cAMP) assay. We observed a 5-fold increase in activation in coGHCR-treated compared with GHCR-treated mice (Figure 1H). The maximum spectral sensitivity of retinas treated with coGHCR was around 500 nm, and a photoresponse was obtained even upon stimulation with light with a wavelength > 600 nm (Figure 1I).

Restoration of visual cortex responses by GHCR

To investigate whether retinal light responses were transmitted to the visual cortex, we then examined visual evoked potentials (VEPs) generated by the visual cortex (Figure 2A). The output from the RGCs is sent through their axons (optic nerve) to the lateral geniculate nucleus (LGN) of the thalamus, which is a region of the diencephalon, then from the LGN to the primary visual cortex in the occipital lobe of the cerebral cortex. For these experiments, we used *rd1* mice in which both eyes had been treated with the AAV-DJ-CAGGS-GHCR, AAV-DJ-CAGGS-coGHCR, or control EGFP (AAV-DJ-CAGGS-EGFP) vectors. Significant VEPs were not detected in the control or GHCR-treated mice. In contrast, VEPs were observed in coGHCR-treated mice (Figure 2B). In response to 3 cd s/m^2 light stimulation, the average VEP amplitude in coGHCR-treated mice was significantly higher (56.4 μV; n = 6) than those in GHCR-treated mice (22.1 μV; n = 8) and control mice (17.9 μV; n = 6) (Figure 2C). Based on this result, all subsequent experiments were performed using coGHCR.

Characterization of the *in vivo* responses restored by GHCR transduction

Next, light-dark transition (LDT) testing was performed to investigate whether ectopic expression of coGHCR in degenerating retinas led to behavioral changes due to vision restoration (Figure 3A). Rodents with intact vision tend to stay in dark places as they are nocturnal and feel uneasy in bright environments, whereas blind rodents spend roughly half of their time in bright places. The coGHCR-treated mice spent significantly less time in the bright area compared with the untreated *rd1* mutant mice (Figure 3B), thereby confirming vision restoration via behavioral analysis. And the visual restoration effect was still maintained after two years (Figure 3C). Furthermore, in order to directly compare the effects of coGHCR with genes in clinical trials, we treated *rd1* mice with chimeric rhodopsin (AAV-6-CAGGS-coGHCR), microbial opsin (AAV-6-CAGGS-ChrimsonR[32]), animal rhodopsin (AAV-6-CAGGS-human rhodopsin), or the control EGFP (AAV-6-CAGGS-EGFP) vector. At an illuminance of 3,000 lux, a significant reduction in the time spent in the bright half of the observation area was noted for coGHCR-treated mice (0.32; n = 6) compared with control mice (0.50; n = 8) (Figure 3D). A similar tendency was observed in ChrimsonR-treated mice

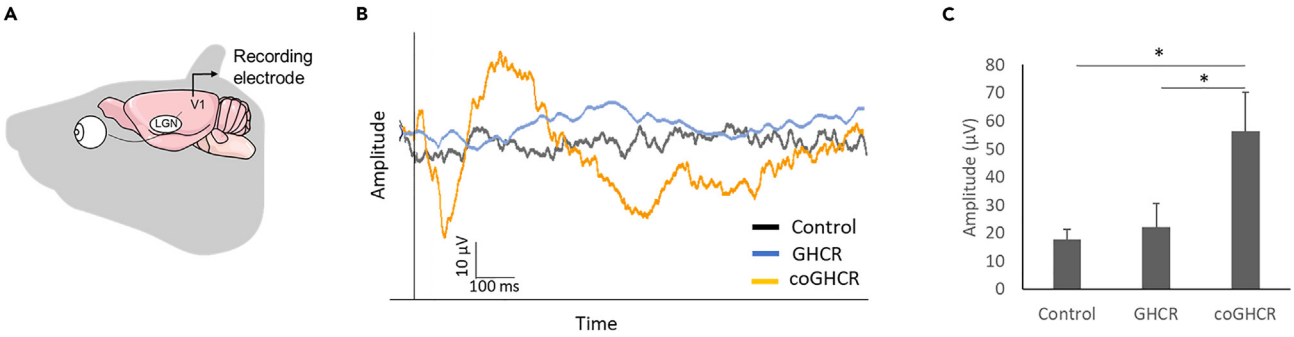

Figure 2. coGHCR restored vision in *rd1* mice through the primary visual cortex

(A) Schematic view of the VEP recording strategy.

(B) Representative VEP traces from GHCR-treated, coGHCR-treated, and control mice.

(C) The average amplitude of the VEPs in the control (AAV-DJ-CAGGS-EGFP, n = 6), GHCR-treated (AAV-DJ-CAGGS-GHCR, n = 8), and coGHCR-treated (AAV-DJ-CAGGS-coGHCR, n = 6) mice. The stimulus was a white LED flash (3 cd s/m^2). Signals were low-pass filtered at 300 Hz and averaged over 60 trials. Error bars represent the SEM. Data were analyzed with one-way ANOVA and Tukey's multiple comparison test; * represents $p \leq 0.05$. V1, visual cortex; LGN, lateral geniculate nucleus; GHCR, *Gloeobacter* and human chimeric rhodopsin; coGHCR, codon-optimized *Gloeobacter* and human chimeric rhodopsin.

(0.36; n = 6). However, no obvious change was observed in human rhodopsin-treated mice (0.48; n = 6). When the experiment was carried out at an illumination of 10 lux, human rhodopsin-treated mice showed a significant change in the time spent in the bright area (0.40; n = 6), whereas ChrimsonR-treated mice did not show an obvious change (0.55; n = 6) (Figure 3E). The coGHCR-treated mice again spent significantly less time in the bright area illuminated at 10 lux (0.40; n = 6).

Restored object recognition function upon GHCR gene therapy

LDT testing measures only light and dark discrimination. Visual recognition testing (VRT) was performed to evaluate whether the mice could recognize an object with the restored level of vision. Mice use vision for their cognitive functions, and are attracted to fighting videos.[33–35] We examined mice in a place preference apparatus with a tablet showing a fighting video (Figure 3F). The ratio of the time spent in the area with the fighting compared with the time spent in the control area (showing a video of an empty cage with the same illuminance) over 15 min was measured. The coGHCR-treated (AAV-DJ-CAGGS-coGHCR) mice spent significantly more time in the fighting video half of the apparatus (0.55, n = 33) than the untreated *rd1* mice (0.50, n = 30). On the other hand, microbial opsin-treated (AAV-DJ-CAGGS-C1V1[36]) mice spent roughly equivalent time in each half (0.49, n = 20) (Figure 3G).

GHCR protective effects against retinal degeneration

We employed another mouse model of retinal degeneration using *Rho*$^{P23H/+}$ mice with the P23H *RHO* mutation, referred to as P23H mice.[37] P23H mice were selected to evaluate the protective effect because they have slower retinal degeneration than *rd1* mice. We subretinally delivered AAV DJ-CAGGS-coGHCR and the control (AAV DJ-CAGGS-EGFP) vector into postnatal day (PND) 0–1 *Rho*$^{P23H/+}$ mouse retinas, targeting the outer retina, and quantified the protective effects of the vector via morphological and electrophysiological examination. Subretinal injection of AAV-DJ efficiently induced gene expression in the murine outer retina (Figure 4A). Optical coherence tomography (OCT) showed that the outer retinal thickness (ORT), which is the thickness from the outer nuclear layer (ONL) to the rod outer segment (ROS), of coGHCR-treated mice (50.0 μm; n = 13) was significantly greater than that of the control mice (42.7 μm; n = 10) at PND 30 (Figures 4B and 4C). The ORT of the treated mice remained significantly greater than that of control mice until PND 50 (Figure S3).

Electroretinography (ERG) revealed that the treated mice had larger rod, mixed, and cone response amplitudes (141.2 μV, 271.4 μV, and 159.0 μV, respectively; n = 9) than the control mice (70.4 μV, 158.7 μV, and 99.1 μV, respectively; n = 14) at PND 30 (Figures 4D and 4E). All amplitudes in the control mice gradually decreased, whereas all amplitudes in the coGHCR-treated mice continued to increase until PND 42 (Figures S4A–S4C). Thereafter, the amplitudes in the treated mice also gradually decreased, although they remained significantly higher than those in the control mice until PND 66.

We also performed terminal deoxynucleotidyl transferase dUTP nick end labeling (TUNEL) to detect apoptosis in the retinas. The number of TUNEL-positive cells in the coGHCR-treated mouse ONL (67.3 cells; n = 3) was significantly lower than that in the control mouse ONL (289.7 cells; n = 3) at PND 31 (Figures 5A–5C).

To expand these observations, we obtained transmission electron microscopy (TEM) images of transverse sections from PND 31 mice. Consistent with the OCT results, the ONL (Figure 5D) and ROS (Figure 5E) of coGHCR-treated mice were relatively intact compared with those of controls, and the ROS structure was less disorganized (Figure 5F). In addition, coGHCR-treated mice had less swelling of their ER, a feature that is indicative of ER stress (Figure 5G).

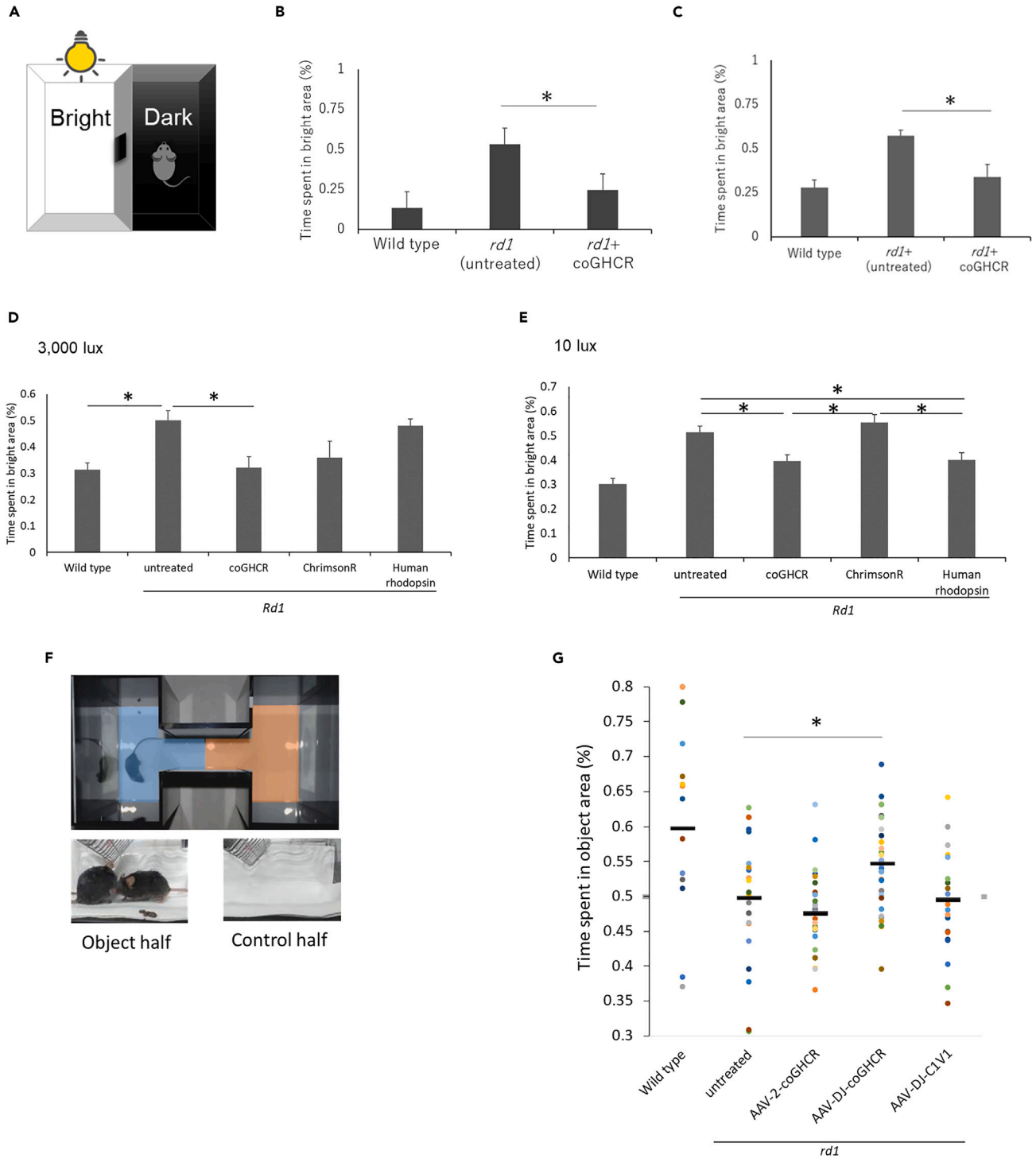

Figure 3. coGHCR-treated mouse behavior indicated vision restoration

(A) LDT testing schematic. Mice were tested in a 30 × 45 × 30-cm box with equally sized bright and dark chambers connected by a 5 × 5-cm opening, across which the mice could move freely.

(B and C) Percentage of time spent in the bright area (total, 10 min) by wild type (n = 4), and control (AAV-DJ-CAGGS-EGFP) (n = 7 in (B) and n = 4 in (C)) and coGHCR-treated (AAV-DJ-CAGGS-coGHCR) *rd1* mice (n = 6). LDT test at 3 months (B) and 2 years (C) after treatment, 10 lux illumination.

Figure 3. *Continued*

(D and E) The percentage of time spent in the bright area (total, 10 min) by wild type (n = 6), and control (AAV-6-CAGGS-EGFP) (n = 8), coGHCR-treated (AAV-6-CAGGS-coGHCR) (n = 6), ChrimsonR-treated (AAV-6-CAGGS-ChrimsonR) (n = 6), and human rhodopsin-treated (AAV-6-CAGGS-human-rhodopsin) *rd1* mice (n = 6). LDT test with 3,000 lux (D) and 10 lux (E) illumination.

(F) VRT setup. Time spent in areas showing a video of mice fighting (object half, blue) or an empty cage (control half, red) was measured.

(G) Distribution of time spent in the object half by wild type (n = 14), and control (no treatment) (n = 23), AAV-2-coGHCR-treated (AAV-2-CAGGS-coGHCR) (n = 30), AAV-DJ-coGHCR-treated (AAV-DJ-CAGGS- coGHCR) (n = 33), and AAV-DJ-C1V1-treated (AAV-DJ-CAGGS-C1V1) *rd1* mice (n = 20). LDT test with 10 lux (D) and 3,000 lux (E) illumination. Black line, average value. Error bars represent the SEM. Data were analyzed with one-way ANOVA and Tukey's multiple comparison test; * represents $p \leq 0.05$. coGHCR, codon-optimized Gloeobacter and human chimeric rhodopsin.

Since retinoid levels are known to affect ER stress and retinal degeneration, retinoid analysis of the treated eyes was performed. The amount of retinal was measured by HPLC using the retinal oxime method after 10 min of exposure to 1000 lux, a fluorescent lighting level assuming a normal indoor environment. The results showed that 11-cis retinal oximes was significantly elevated in the treated eyes (54.1 $\pm$ 18.2 pmol/2 retinas; n = 9) versus controls (39.5 $\pm$ 6.5 pmol/2 retinas; n = 9) (Figures 5H and 5I). The amount of all-trans-retinal oxime was also elevated in treated eyes; however, this elevation did not attain statistical significance (p = 0.22) (Figure 5J).

DISCUSSION

Because the phenotype of retinal degeneration is common across cases of RP, regardless of genotype, the strategy of optogenetic therapy has great potential as a universal therapeutic approach. It aims to target non-photoreceptive surviving neurons in the retina, such as RGCs and bipolar cells, and convert them to photoreceptive.

In this study, we demonstrated that ectopic expression of coGHCR is an effective method of optogenetic vision restoration in mice with retinal degeneration. MEA revealed that photoresponses were maintained for retinal irradiance levels as low as 10^{13} photons/cm^2/s. This is consistent with the response of the treated mice to 10 lux illumination in the behavioral test, and represents a significant improvement in sensitivity compared with that observed in previous studies of vision restoration with microbial opsins (threshold: 10^{14} to 10^{17} photons/cm^2/s),[2–7] LiGluR/MAG photoswitches (threshold: 10^{15}–10^{16} photons/cm^2/s),[38,39] or photoactivated ligands (AAQ threshold: 10^{15} photons/cm^2/s[40] and DENAQ threshold: 4×10^{13} photons/cm^2/s[41]). Although some vectors restored greater sensitivity, such as human rhodopsin,[9] cone opsin,[16] and Opto-mgluR6 (10^{12} photons/cm^2/s),[8] our LDT results at 3,000 lux (similar to a cloudy outdoor environment) suggest that photobleaching of rhodopsin like these does not work in bright environments. coGHCR is adaptable to a light environment ranging from at least 10 lux (similar to a night light levels with streetlights) to 3,000 lux, and is, thus, a suitable single-opsin vision restoration tool.

Furthermore, the typical channelrhodopsins have a spectrum limited to blue light,[42] which limits their use as a visual restoration tool. On the other hand, GHCR has a spectrum peak around 500 nm and facilitates responses to red light. Irradiation of high-energy light such as blue light can cause phototoxicity and cell death due to generation of free radicals.[43] Therefore, there are concerns about phototoxicity in optogenetic tools that operate under blue light, such as channelrhodopsin, and long wavelength-shifted opsins have been developed.[44] In this regard, the GHCR has the advantage of being highly sensitive and having a peak at intermediate (green) wavelengths, making it responsive to short and long wavelengths and less likely to exceed safe limits of light intensity.[45] In addition, behavioral tests showed that coGHCR enabled responses to both sustained and transient stimulation lasting 10 ms. These findings suggested that coGHCR gene therapy can restore sensitivity to multiple light environments encountered in daily life.

The ERG amplitudes in coGHCR-treated mice continued to increase until PND 42, likely because the coGHCR-mediated signal was additive with the innate amplitude. This is consistent with the fact that gene expression of the AAV-DJ vector peaks at approximately 1.5 months after administration.[25] We observed no apparent changes in the shapes of the ERG waveforms in the coGHCR-treated mice. The visual restoration effect was also maintained for two years, which shows promise for long-term pharmacological effects and safety.

coGHCR has Gt activity derived from rhodopsin.[24] Gt is also known to be cross-linked with Gi/o,[46] and this was confirmed (Figure 1H). Although this study used a ubiquitous promoter, which cannot be fully confirmed, Gi/o is generally expressed specifically in ON-type bipolar cells,[47,48] where the light-responsive signal is likely to have been generated. When coGHCR is expressed ectopically in ON bipolar cells, it is expected to inhibit responses. However, the restored responses observed by MEA were all ON responses. In addition, the electrophysiological and behavioral results were similar to physiological responses, and no reversal reaction observed. In *rd1* mice, photoreceptors are mostly lost by 4 weeks after birth and no optical response is obtained after 7 weeks at the latest.[49,50] Therefore, responses from residual photoreceptors are unlikely in this study. A similar phenomenon has been confirmed in previous studies; the excitatory response is hypothesized to result from disinhibition of inhibitory amacrine cells.[6,8,9]

The safety of ectopic expression of opsins, such as channelrhodopsin 2, has been previously reported.[3,51,52] To our knowledge, this is the first report of their protective effects against retinal degeneration. *In vitro* studies have shown that the P23H opsin is misfolded and retained in the ER.[53] ER retention of P23H opsin can induce the unfolded protein response, leading to apoptosis.[54–57] Our results suggest that expression of coGHCR in the retinal outer layer suppressed photoreceptor apoptosis, which led to protection against degeneration. The lack of 11-cis-retinal induces cytotoxicity during the development of ROS in P23H mice.[58] In fact, the amount of *cis*-retinal in the retina was significantly elevated after coGHCR treatment. Since coGHCR uses all-trans retinal as a chromophore, like microbial opsin, it does not consume *cis*-retinal and is free from photobleaching. Therefore, the expressed coGHCR may suppress *cis*-retinal consumption via photoreceptor substitution. If this hypothesis is correct, the protection effect of coGHCR may not be applicable to patients with all IRD

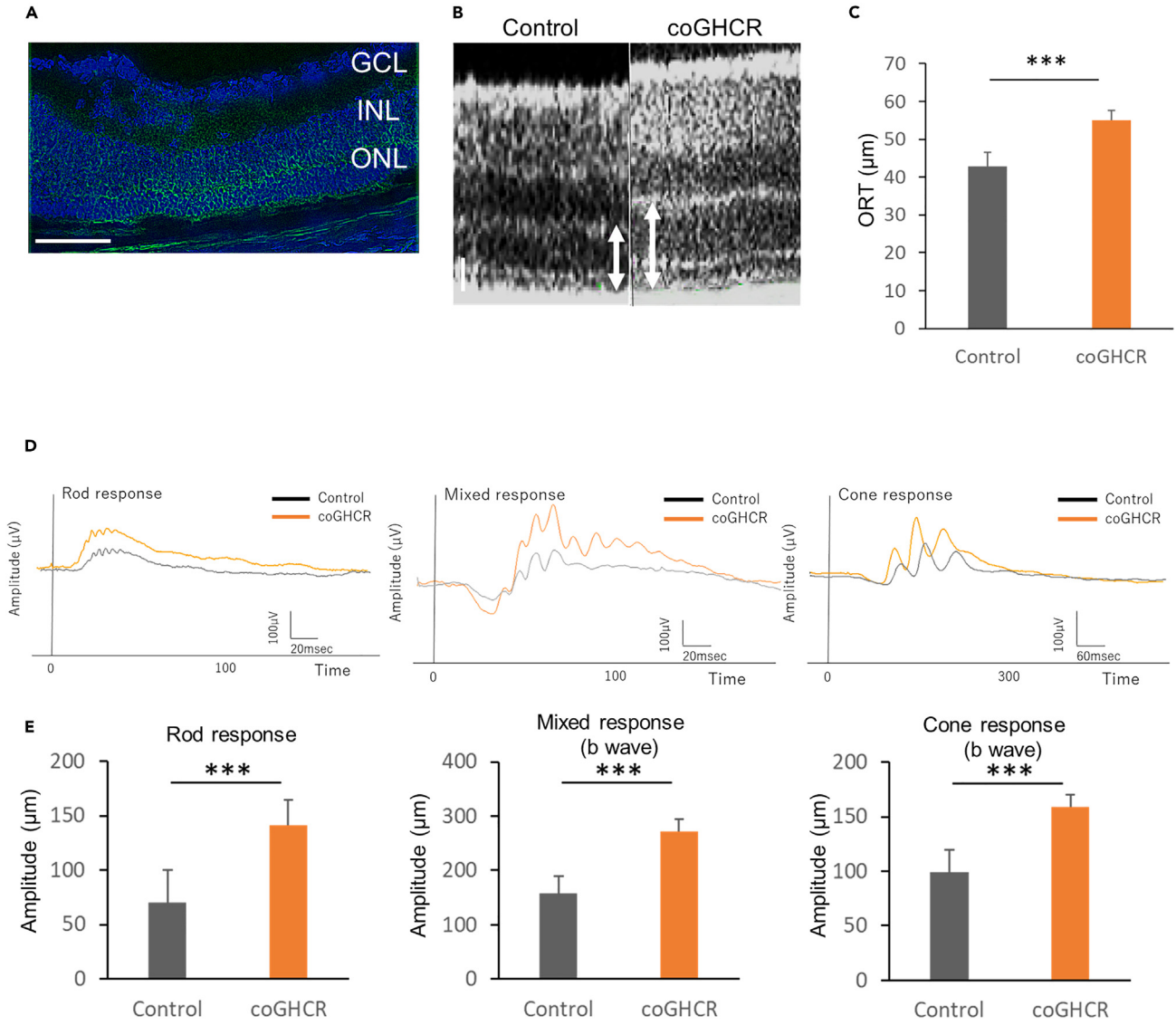

Figure 4. Ectopic coGHCR expression protects against photoreceptor degeneration

(A) Confocal image of a transverse section through the P23H retina 2 months after AAV-DJ-CAGGS-coGHCR subretinal injection. Green, FLAG tag fused to the C-terminus of coGHCR; blue, DAPI nuclear counterstaining. Scale bar, 100 μm.

(B) OCT retinal image sections from coGHCR-treated and control (AAV-DJ-CAGGS-EGFP subretinally injected) mice at PND 30. The white arrow indicates the measured ORT (from ONL to cone outer segment). Scale bar, 20 μm.

(C) Histogram of the measured ORT of the coGHCR-treated (n = 13) and control mice (n = 10) at PND 30.

(D and E) Representative ERG waveforms (rod response, mixed response, and cone response) of coGHCR-treated (n = 14) and control mice (n = 9) (D). Histograms of the average ERG amplitudes from panel d at PND 30 (E). Error bars represent SEM. Data were analyzed with the unpaired t-test; *** represents $p \leq 0.001$. GCL, ganglion cell layer; INL, inner nuclear layer; ONL, outer nuclear layer; GHCR, coGHCR, codon-optimized *Gloeobacter* and human chimeric rhodopsin; ORT, outer retinal thickness.

genotypes. However, there are more than 140 known RP-linked rhodopsin mutations, and those that result in protein misfolding and retention in the ER are the most prevalent.[59,60]

In summary, the coGHCR vector has the advantages of both animal and microbial opsin as a vision regeneration tool. It restores sensitivity and an action spectrum that enables vision in lighting ranging from levels found outdoors to those in dimly lit indoor environments via G protein stimulation without the risk of bleaching; it can also be expected to protect against the progression of retinal degeneration in the majority of IRD patients. These results suggest that coGHCR is worthy of consideration for clinical application as a gene therapy for IRD.

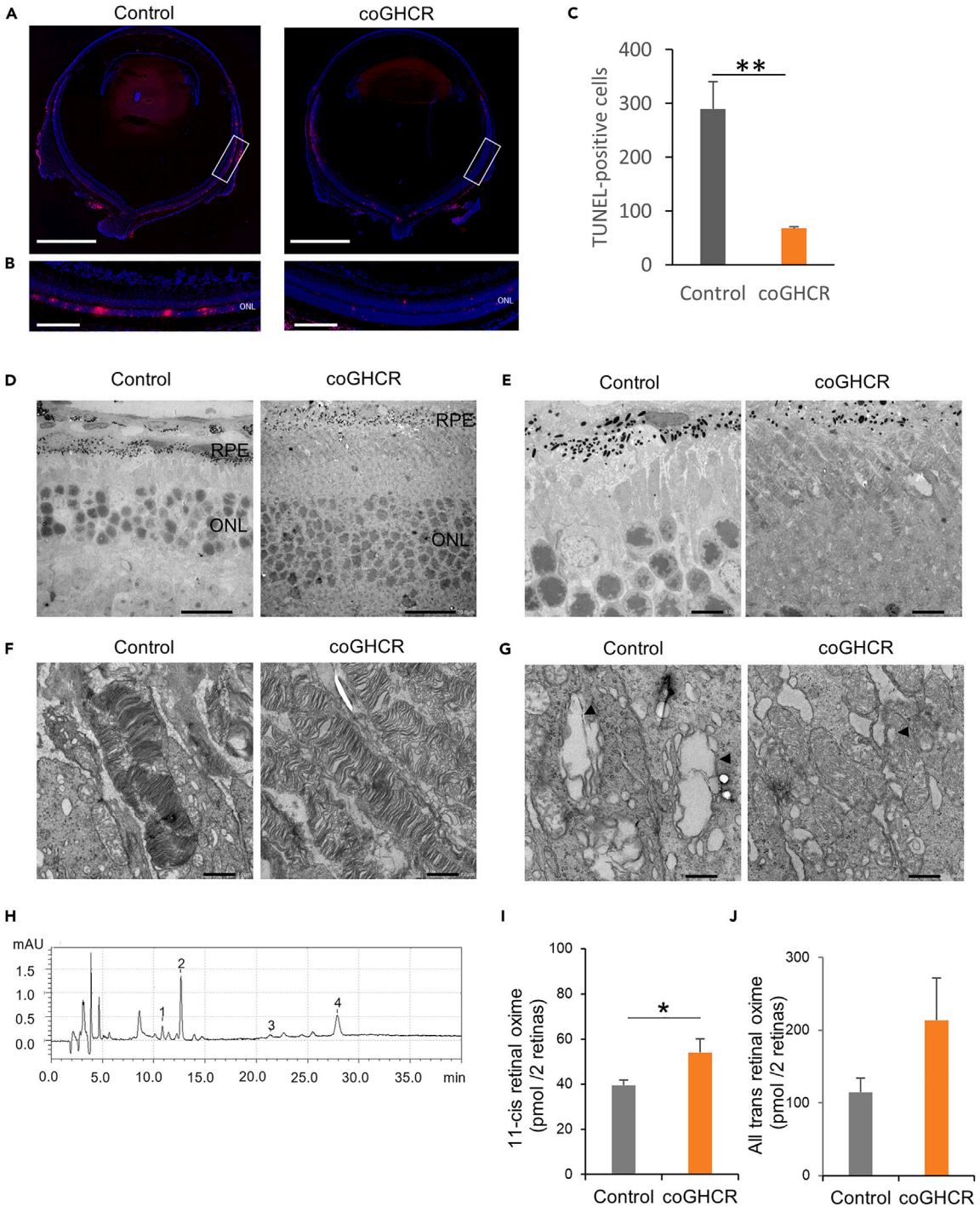

Figure 5. coGHCR treatment suppressed retinal apoptosis and ER stress

(A and B) TUNEL-stained transverse sections (A) and enlarged images of the white squares (B) of coGHCR-treated and control (AAV-DJ-CAGGS-EGFP subretinally injected) mouse retinas at PND 31. Red, TUNEL-positive cells; blue, DAPI nuclear counterstaining. Scale bar, 1,000 μm in (a) and 100 μm in (B).

(C) Histogram of the number of TUNEL-positive cells in the ONLs of coGHCR-treated (n = 3) and control mice (n = 3) at PND 31.

(D–G) (D) TEM images of transverse sections from coGHCR-treated and control mice at PND 31, showing the outer retinal layer (D), the outer segment at low magnification (E) and high magnification (F), and the inner segment (G). The arrowhead indicates swollen ER. Scale bar, 20 μm in (D), 5 μm in (E), 1 μm in (F), and 500 nm in (G).

Figure 5. *Continued*

(H) Chromatograms of retinal in mouse retina analyzed by HPLC. 15 h dark adapted mice were exposed to light of 1000 lux for 10 min and each retina was processed and retinal oximes extracted under dim red light. Peak identification was determined using retinal standard reagents as follows: 1, syn-11-cis-retinal oxime; 2, syn-all-trans-retinal oxime; 3, anti-11-cis-retinal oxime; 4, anti-all-trans-retinal oxime.

(I and J) Histogram quantifying the amount of retinal oximes from coGHCR-treated (n = 9) and control mice (n = 9) obtained from HPLC. Error bars represent SEM. Data were analyzed with the unpaired t-test; * represents $p \leq 0.05$, ** represents $p \leq 0.01$. coGHCR, codon-optimized *Gloeobacter* and human chimeric rhodopsin; RPE, retinal pigment epithelium; ONL, outer nuclear layer.

Limitations of the study

In this study, a protective effect on IRD was observed, suggesting that ER stress and changes in retinal composition are involved. On the other hand, this was the result in $Rho^{P23H/+}$ mice, and it is not clear whether this is applicable to other genotypes of IRD, and further studies are needed to determine the exact mechanism.

STAR★METHODS

Detailed methods are provided in the online version of this paper and include the following:

- KEY RESOURCES TABLE
- RESOURCE AVAILABILITY
  - Lead contact
  - Materials availability
  - Data and code availability
- EXPERIMENTAL MODEL AND STUDY PARTICIPANT DETAILS
  - Study approval
- METHOD DETAILS
  - Immunohistochemistry
  - Vector production and purification
  - Virus injection
  - Multielectrode array recordings
  - ERG analyses
  - VEP analyses
  - LDT recording
  - VRT recording
  - Gi/o coupled GPCR activation assay
  - TEM
  - Preparation of cryosections of retinas
  - TUNEL assay
  - OCT imaging
  - HPLC analysis of retinal
  - Data and software availability
- QUANTIFICATION AND STATISTICAL ANALYSIS

SUPPLEMENTAL INFORMATION

Supplemental information can be found online at https://doi.org/10.1016/j.isci.2023.107716.

ACKNOWLEDGMENTS

Y.K. is supported by grants from the Keio University Doctorate Student Grant-in-Aid Program. T.K. is supported by Grants-in-Aid from Takeda Science Foundation and the Keio University Medical Science Fund. This work was also supported by AMED under grant Number JP21ek0109526h0001 JP22gm1510007, JSPS KAKENHI grant Numbers JP19K24053, JP21K16907, JP23K15939. We would like to thank Editage (www.editage.com) for English language editing.

AUTHOR CONTRIBUTIONS

Y.K. and T.K. designed the research, wrote the manuscript. Y.K. performed the retinal histology, MEA, ERG and VEP recordings, and WB, TEM, LDT and VRT experiments. N.S. performed HPLC. K.Y. performed plasmid construction. K.K. performed AAV production. Y.K. performed data processing and analysis. K.N., D.L., H.K., H.O and T.K. made critical revisions of the manuscript. T.K. supervised the research.

DECLARATION OF INTERESTS

Y.K., H.K., K.T., and T.K. are inventors on pending patents (PCT/JP2017/031579、PCT/JP2019/1565) related to this work. Y.K. is CEO of Restore Vision Inc.

INCLUSION AND DIVERSITY

We support inclusive, diverse, and equitable conduct of research.

Received: May 10, 2023
Revised: July 22, 2023
Accepted: August 22, 2023
Published: August 25, 2023

REFERENCES

1. Sahel, J.-A., Marazova, K., and Audo, I. (2014). Clinical characteristics and current therapies for inherited retinal degenerations. Cold Spring Harb. Perspect. Med. *5*, a017111. https://doi.org/10.1101/cshperspect.a017111.
2. Bi, A., Cui, J., Ma, Y.P., Olshevskaya, E., Pu, M., Dizhoor, A.M., and Pan, Z.H. (2006). Ectopic Expression of a Microbial-Type Rhodopsin Restores Visual Responses in Mice with Photoreceptor Degeneration. Neuron *50*, 23–33. https://doi.org/10.1016/j.neuron.2006.02.026.
3. Doroudchi, M.M., Greenberg, K.P., Liu, J., Silka, K.A., Boyden, E.S., Lockridge, J.A., Arman, A.C., Janani, R., Boye, S.E., Boye, S.L., et al. (2011). Virally delivered Channelrhodopsin-2 Safely and Effectively Restores Visual Function in Multiple Mouse Models of Blindness. Mol. Ther. *19*, 1220–1229. https://doi.org/10.1038/MT.2011.69.
4. Lagali, P.S., Balya, D., Awatramani, G.B., Münch, T.A., Kim, D.S., Busskamp, V., Cepko, C.L., and Roska, B. (2008). Light-activated channels targeted to ON bipolar cells restore visual function in retinal degeneration. Nat. Neurosci. *11*, 667–675. https://doi.org/10.1038/nn.2117.
5. Cronin, T., Vandenberghe, L.H., Hantz, P., Juttner, J., Reimann, A., Kacsó, A.E., Huckfeldt, R.M., Busskamp, V., Kohler, H., Lagali, P.S., et al. (2014). Efficient transduction and optogenetic stimulation of retinal bipolar cells by a synthetic adeno-associated virus capsid and promoter. EMBO Mol. Med. *6*, 1175–1190. https://doi.org/10.15252/emmm.201404077.
6. Macé, E., Caplette, R., Marre, O., Sengupta, A., Chaffiol, A., Barbe, P., Desrosiers, M., Bamberg, E., Sahel, J.-A., Picaud, S., et al. (2014). Targeting channelrhodopsin-2 to ON-bipolar cells with vitreally administered AAV restores ON and OFF visual responses in blind mice. Mol. Ther. *23*, 7–16. https://doi.org/10.1038/mt.2014.154.
7. Busskamp, V., Duebel, J., Balya, D., Fradot, M., Viney, T.J., Siegert, S., Groner, A.C., Cabuy, E., Forster, V., Seeliger, M., et al. (2010). Genetic Reactivation of Cone Photoreceptors Restores Visual Responses in Retinitis Pigmentosa. Science *329*, 413–417. https://doi.org/10.1126/science.1190897.
8. Van Wyk, M., Pielecka-Fortuna, J., Löwel, S., and Kleinlogel, S. (2015). Restoring the ON Switch in Blind Retinas: Opto-mGluR6, a Next-Generation, Cell- Tailored Optogenetic Tool. PLoS Biol. *13*, e1002143.
9. Pienaar, A., Bedford, R., Davis, K., and Bishop, P.N. (2015). Restoration of vision with ectopic expression of human rod opsin. Curr. Biol. *25*, 1–35. https://doi.org/10.1016/j.cub.2015.07.029.
10. Sahel, J.A., Boulanger-Scemama, E., Pagot, C., Arleo, A., Galluppi, F., Martel, J.N., Esposti, S.D., Delaux, A., de Saint Aubert, J.B., de Montleau, C., et al. (2021). Partial recovery of visual function in a blind patient after optogenetic therapy. Nat. Med. *27*, 1223–1229. https://doi.org/10.1038/s41591-021-01351-4.
11. Kleinlogel, S., Feldbauer, K., Dempski, R.E., Fotis, H., Wood, P.G., Bamann, C., and Bamberg, E. (2011). Ultra light-sensitive and fast neuronal activation with the Ca^{2}+-permeable channelrhodopsin CatCh. Nat. Neurosci. *14*, 513–518. https://doi.org/10.1038/nn.2776.
12. Kleinlogel, S., Terpitz, U., Legrum, B., Gökbuget, D., Boyden, E.S., Bamann, C., Wood, P.G., and Bamberg, E. (2011). A gene-fusion strategy for stoichiometric and co-localized expression of light-gated membrane proteins. Nat. Methods *8*, 1083–1088. https://doi.org/10.1038/nmeth.1766.
13. Pan, Z.H., Ganjawala, T.H., Lu, Q., Ivanova, E., and Zhang, Z. (2014). ChR2 mutants at L132 and T159 with improved operational light sensitivity for vision restoration. PLoS One *9*, e98924.
14. Grimm, C., Wenzel, A., Hafezi, F., Yu, S., Redmond, T.M., and Remé, C.E. (2000). Protection of Rpe65-deficient mice identifies rhodopsin as a mediator of light-induced retinal degeneration. Nat. Genet. *25*, 63–66. https://doi.org/10.1038/75614.
15. Vaughan, D.K., Coulibaly, S.F., Darrow, R.M., and Organisciak, D.T. (2003). A morphometric study of light-induced damage in transgenic rat models of retinitis pigmentosa. Invest. Ophthalmol. Vis. Sci. *44*, 848–855. https://doi.org/10.1167/iovs.02-0709.
16. Berry, M.H., Holt, A., Salari, A., Veit, J., Visel, M., Levitz, J., Aghi, K., Gaub, B.M., Sivyer, B., Flannery, J.G., and Isacoff, E.Y. (2019). Restoration of high-sensitivity and adapting vision with a cone opsin. Nat. Commun. *10*, 1221. https://doi.org/10.1038/s41467-019-09124-x.
17. Rózanowska, M., and Sarna, T. (2005). Light-induced Damage to the Retina: Role of Rhodopsin Chromophore Revisited. Photochem. Photobiol. *81*, 1305–1330. https://doi.org/10.1562/2004-11-13-ir-371.
18. Maeda, A., Maeda, T., Golczak, M., Chou, S., Desai, A., Hoppel, C.L., Matsuyama, S., and Palczewski, K. (2009). Involvement of all-trans-retinal in acute light-induced retinopathy of mice. J. Biol. Chem. *284*, 15173–15183. https://doi.org/10.1074/jbc.M900322200.
19. Hickey, D.G., Davies, W.I.L., Hughes, S., Rodgers, J., Thavanesan, N., MacLaren, R.E., and Hankins, M.W. (2021). Chimeric human opsins as optogenetic light sensitisers. J. Exp. Biol. *224*, jeb240580.
20. Rodgers, J., Bano-Otalora, B., Belle, M.D.C., Paul, S., Hughes, R., Wright, P., McDowell, R., Milosavljevic, N., Orlowska-Feuer, P., Martial, F.P., et al. (2021). Using a bistable animal opsin for switchable and scalable optogenetic inhibition of neurons. EMBO Rep. *22*, e51866.
21. Mure, L.S., Cornut, P.L., Rieux, C., Drouyer, E., Denis, P., Gronfier, C., and Cooper, H.M. (2009). Melanopsin Bistability: A Fly's Eye Technology in the Human Retina. PLoS One *4*, e5991. https://doi.org/10.1371/JOURNAL.PONE.0005991.
22. Geiser, A.H., Sievert, M.K., Guo, L.-W., Grant, J.E., Krebs, M.P., Fotiadis, D., Engel, A., and Ruoho, A.E. (2006). Bacteriorhodopsin chimeras containing the third cytoplasmic loop of bovine rhodopsin activate transducin for GTP/GDP exchange. Protein Sci. *15*, 1679–1690. https://doi.org/10.1110/ps.062192306.
23. Nakatsuma, A., Yamashita, T., Sasaki, K., Kawanabe, A., Inoue, K., Furutani, Y., Shichida, Y., and Kandori, H. (2011). Chimeric microbial rhodopsins containing the third cytoplasmic loop of bovine rhodopsin. Biophys. J. *100*, 1874–1882. https://doi.org/10.1016/j.bpj.2011.02.054.
24. Sasaki, K., Yamashita, T., Yoshida, K., Inoue, K., Shichida, Y., and Kandori, H. (2014). Chimeric Proton-Pumping Rhodopsins Containing the Cytoplasmic Loop of Bovine Rhodopsin. PLoS One *9*, e91323. https://doi.org/10.1371/journal.pone.0091323.
25. Katada, Y., Kobayashi, K., Tsubota, K., and Kurihara, T. (2019). Evaluation of AAV-DJ Vector for Retinal Gene Therapy. PeerJ *7*, e6317.
26. Grimm, D., Lee, J.S., Wang, L., Desai, T., Akache, B., Storm, T.A., and Kay, M.A. (2008). *In vitro* and *in vivo* gene therapy vector evolution via multispecies interbreeding and retargeting of adeno-associated viruses. J. Virol. *82*, 5887–5911. https://doi.org/10.1128/JVI.00254-08.
27. Keeler, A.M., and Flotte, T.R. (2019). Recombinant Adeno-Associated Virus Gene Therapy in Light of Luxturna (and Zolgensma and Glybera): Where Are We, and How Did We Get Here? Annu. Rev. Virol. *6*, 601–621.
28. Bailes, H.J., and Lucas, R.J. (2013). Human melanopsin forms a pigment maximally sensitive to blue light (λmax ≈ 479 nm) supporting activation of Gq/11 and Gi/o signalling cascades. Proc. R. Soc. B Biol. Sci. *280*, 20122987.

29. Li, X., Gutierrez, D.V., Hanson, M.G., Han, J., Mark, M.D., Chiel, H., Hegemann, P., Landmesser, L.T., and Herlitze, S. (2005). Fast noninvasive activation and inhibition of neural and network activity by vertebrate rhodopsin and green algae channelrhodopsin. Proc. Natl. Acad. Sci. USA *102*, 17816–17821. https://doi.org/10.1073/pnas.0509030102.
30. Gutierrez, D.V., Mark, M.D., Masseck, O., Maejima, T., Kuckelsberg, D., Hyde, R.A., Krause, M., Kruse, W., and Herlitze, S. (2011). Optogenetic control of motor coordination by G i/o protein-coupled vertebrate rhodopsin in cerebellar purkinje cells. J. Biol. Chem. *286*, 25848–25858. https://doi.org/10.1074/jbc.M111.253674.
31. Cao, P., Sun, W., Kramp, K., Zheng, M., Salom, D., Jastrzebska, B., Jin, H., Palczewski, K., and Feng, Z. (2012). Light-sensitive coupling of rhodopsin and melanopsin to G i/o and G q signal transduction in Caenorhabditis elegans. FASEB J *26*, 480–491. https://doi.org/10.1096/fj.11-197798.
32. Klapoetke, N.C., Murata, Y., Kim, S.S., Pulver, S.R., Birdsey-Benson, A., Cho, Y.K., Morimoto, T.K., Chuong, A.S., Carpenter, E.J., Tian, Z., et al. (2014). Independent optical excitation of distinct neural populations. Nat. Methods *11*, 338–346. https://doi.org/10.1038/nmeth.2836.
33. Watanabe, S., Shinozuka, K., and Kikusui, T. (2016). Preference for and discrimination of videos of conspecific social behavior in mice. Anim. Cogn. *19*, 523–531. https://doi.org/10.1007/s10071-016-0953-x.
34. Watanabe, S. (2013). Preference for and Discrimination of Paintings by Mice. PLoS One *8*, e65335.
35. Yakura, T., Yokota, H., Ohmichi, Y., Ohmichi, M., Nakano, T., and Naito, M. (2018). Visual recognition of mirror, video-recorded, and still images in rats. PLoS One *13*, e0194215.
36. Erbguth, K., Prigge, M., Schneider, F., Hegemann, P., and Gottschalk, A. (2012). Bimodal Activation of Different Neuron Classes with the Spectrally Red-Shifted Channelrhodopsin Chimera C1V1 in Caenorhabditis elegans. PLoS One *7*, e46827.
37. Sakami, S., Kolesnikov, A.V., Kefalov, V.J., and Palczewski, K. (2014). P23H opsin knock-in mice reveal a novel step in retinal rod disc morphogenesis. Hum. Mol. Genet. *23*, 1723–1741. https://doi.org/10.1093/hmg/ddt561.
38. Caporale, N., Kolstad, K.D., Lee, T., Tochitsky, I., Dalkara, D., Trauner, D., Kramer, R., Dan, Y., Isacoff, E.Y., and Flannery, J.G. (2011). LiGluR restores visual responses in rodent models of inherited blindness. Mol. Ther. *19*, 1212–1219. https://doi.org/10.1038/mt.2011.103.
39. Gaub, B.M., Berry, M.H., Holt, A.E., Reiner, A., Kienzler, M.A., Dolgova, N., Nikonov, S., Aguirre, G.D., Beltran, W.A., Flannery, J.G., et al. (2014). Restoration of Visual Function by Expression of a Light-Gated Mammalian Ion Channel in Retinal Ganglion Cells or ON-Bipolar Cells.
40. Polosukhina, A., Litt, J., Tochitsky, I., Nemargut, J., Sychev, Y., De Kouchkovsky, I., Huang, T., Borges, K., Trauner, D., Van Gelder, R.N., and Kramer, R.H. (2012). Photochemical Restoration of Visual Responses in Blind Mice. Neuron *75*, 271–282. https://doi.org/10.1016/j.neuron.2012.05.022.
41. Tochitsky, I., Polosukhina, A., Degtyar, V.E., Gallerani, N., Smith, C.M., Friedman, A., Van Gelder, R.N., Trauner, D., Kaufer, D., and Kramer, R.H. (2014). Restoring visual function to blind mice with a photoswitch that exploits electrophysiological remodeling of retinal ganglion cells. Neuron *81*, 800–813. https://doi.org/10.1016/j.neuron.2014.01.003.
42. Nagel, G., Szellas, T., Huhn, W., Kateriya, S., Adeishvili, N., Berthold, P., Ollig, D., Hegemann, P., and Bamberg, E. (2003). Channelrhodopsin-2, a directly light-gated cation-selective membrane channel. Proc. Natl. Acad. Sci. USA *100*, 13940–13945. https://doi.org/10.1073/pnas.1936192100.
43. Hunter, J.J., Morgan, J.I.W., Merigan, W.H., Sliney, D.H., Sparrow, J.R., and Williams, D.R. (2012). The susceptibility of the retina to photochemical damage from visible light. Prog. Retin. Eye Res. *31*, 28–42. https://doi.org/10.1016/J.PRETEYERES.2011.11.001.
44. Sengupta, A., Chaffiol, A., Macé, E., Caplette, R., Forster, V., Marre, O., Lin, J.Y., Desrosiers, M., Sahel, J., Picaud, S., et al. (2016). Red-shifted channelrhodopsin stimulation restores light responses in blind mice , macaque retina , and human retina. EMBO Mol. Med. *8*, 1248–1264. https://doi.org/10.15252/emmm.201505699.
45. International Commission on Non-Ionizing Radiation Protection ICNIRP (2013). ICNIRP Guidelines on Limits of Exposure to Laser Radiation of Wavelengths between 180 nm and 1,000 µm. Health Phys. *105*, 271–295. https://doi.org/10.1097/HP.0B013E3182983FD4.
46. Ballister, E.R., Rodgers, J., Martial, F., and Lucas, R.J. (2018). A live cell assay of GPCR coupling allows identification of optogenetic tools for controlling Go and Gi signaling. BMC Biol. *16*, 10. https://doi.org/10.1186/s12915-017-0475-2.
47. Dhingra, A., Jiang, M., Wang, T.-L., Lyubarsky, A., Savchenko, A., Bar-Yehuda, T., Sterling, P., Birnbaumer, L., and Vardi, N. (2002). Light response of retinal ON bipolar cells requires a specific splice variant of Galpha(o). J. Neurosci. *22*, 4878–4884.
48. Hulliger, E.C., Hostettler, S.M., and Kleinlogel, S. (2020). Empowering Retinal Gene Therapy with a Specific Promoter for Human Rod and Cone ON-Bipolar Cells. Mol. Ther. Methods Clin. Dev. *17*, 505–519.
49. Fujii, M., Sunagawa, G.A., Kondo, M., Takahashi, M., and Mandai, M. (2016). Evaluation of micro Electroretinograms Recorded with Multiple Electrode Array to Assess Focal Retinal Function. Sci. Rep. *6*, 30719. https://doi.org/10.1038/srep30719.
50. Chang, B., Hawes, N.L., Pardue, M.T., German, A.M., Hurd, R.E., Davisson, M.T., Nusinowitz, S., Rengarajan, K., Boyd, A.P., Sidney, S.S., et al. (2007). Two mouse retinal degenerations caused by missense mutations in the beta-subunit of rod cGMP phosphodiesterase gene. Vis. Res. *47*, 624–633. https://doi.org/10.1016/j.visres.2006.11.020.
51. Sugano, E., Isago, H., Wang, Z., Murayama, N., Tamai, M., and Tomita, H. (2011). Immune responses to adeno-associated virus type 2 encoding channelrhodopsin-2 in a genetically blind rat model for gene therapy. Gene Ther. *18*, 266–274. https://doi.org/10.1038/gt.2010.140.
52. Ivanova, E., and Pan, Z.H. (2009). Evaluation of the adeno-associated virus mediated long-term expression of channelrhodopsin-2 in the mouse retina. Mol. Vis. *15*, 1680–1689.
53. Chapple, J.P., Grayson, C., Hardcastle, A.J., Saliba, R.S., Van Der Spuy, J., and Cheetham, M.E. (2001). Unfolding retinal dystrophies: A role for molecular chaperones? Trends Mol. Med. *7*, 414–421. https://doi.org/10.1016/S1471-4914(01)02103-7.
54. Liu, X., Garriga, P., and Khorana, H.G. (1996). Structure and function in rhodopsin: Correct folding and misfolding in two point mutants in the intradiscal domain of rhodopsin identified in retinitis pigmentosa. Proc. Natl. Acad. Sci. USA *93*, 4554–4559. https://doi.org/10.1073/pnas.93.10.4554.
55. Frederick, J.M., Krasnoperova, N.V., Hoffmann, K., Church-Kopish, J., Rüther, K., Howes, K., Lem, J., and Baehr, W. (2001). Mutant rhodopsin transgene expression on a null background. Invest. Ophthalmol. Vis. Sci. *42*, 826–833.
56. Leonard, K.C., Petrin, D., Coupland, S.G., Baker, A.N., Leonard, B.C., LaCasse, E.C., Hauswirth, W.W., Korneluk, R.G., and Tsilfidis, C. (2007). XIAP protection of photoreceptors in animal models of retinitis pigmentosa. PLoS One *2*, e314.
57. Lin, J.H., Li, H., Yasumura, D., Cohen, H.R., Zhang, C., Panning, B., Shokat, K.M., LaVail, M.M., and Walter, P. (2007). IRE1 signaling affects cell fate during the unfolded protein response. Science *318*, 944–949. https://doi.org/10.1126/science.1146361.
58. Sakami, S., Maeda, T., Bereta, G., Okano, K., Golczak, M., Sumaroka, A., Roman, A.J., Cideciyan, A.V., Jacobson, S.G., and Palczewski, K. (2011). Probing mechanisms of photoreceptor degeneration in a new mouse model of the common form of autosomal dominant retinitis pigmentosa due to P23H opsin mutations. J. Biol. Chem. *286*, 10551–10567. https://doi.org/10.1074/jbc.M110.209759.
59. Mendes, H.F., Van Der Spuy, J., Chapple, J.P., and Cheetham, M.E. (2005). Mechanisms of cell death in rhodopsin retinitis pigmentosa: Implications for therapy. Trends Mol. Med. *11*, 177–185. https://doi.org/10.1016/j.molmed.2005.02.007.
60. Yoshida, T., Ozawa, Y., Suzuki, K., Yuki, K., Ohyama, M., Akamatsu, W., Matsuzaki, Y., Shimmura, S., Mitani, K., Tsubota, K., and Okano, H. (2014). The use of induced pluripotent stem cells to reveal pathogenic gene mutations and explore treatments for retinitis pigmentosa. Mol. Brain *7*, 45. https://doi.org/10.1186/1756-6606-7-45.
61. Kubota, Y., Hirashima, M., Kishi, K., Stewart, C.L., and Suda, T. (2008). Leukemia inhibitory factor regulates microvessel density by modulating oxygen-dependent VEGF expression in mice. J. Clin. Invest. *118*, 2393–2403. https://doi.org/10.1172/JCI34882.
62. Kurihara, T., Ozawa, Y., Shinoda, K., Nagai, N., Inoue, M., Oike, Y., Tsubota, K., Ishida, S., and Okano, H. (2006). Neuroprotective effects of angiotensin II type 1 receptor (AT1R) blocker, telmisartan, via modulating AT1R and AT2R signaling in retinal inflammation. Invest. Ophthalmol. Vis. Sci. *47*, 5545–5552. https://doi.org/10.1167/iovs.06-0478.

STAR★METHODS

KEY RESOURCES TABLE

REAGENT or RESOURCE	SOURCE	IDENTIFIER
Antibodies		
anti-FLAG	Merck	MAB3118; RRID: AB_94705
anti-PKCα	Abcam	ab32376; RRID: AB_777294
anti-rabbit Alexa TM488	Abcam	ab150077; RRID: AB_2630356
anti-rabbit Alexa TM 594	Abcam	ab150080; RRID: AB_2650602
Bacterial and virus strains		
AAV-2-CAGGS-EGFP	Section of Viral Vector Development, Center for Genetic Analysis of Behavior, National Institute for Physiological Sciences	N/A
AAV-2-CAGGS-coGHCR	Section of Viral Vector Development, Center for Genetic Analysis of Behavior, National Institute for Physiological Sciences	N/A
AAV-DJ-CAGGS-GHCR	Section of Viral Vector Development, Center for Genetic Analysis of Behavior, National Institute for Physiological Sciences	N/A
AAV-DJ-CAGGS-EGFP	Section of Viral Vector Development, Center for Genetic Analysis of Behavior, National Institute for Physiological Sciences	N/A
AAV-DJ-CAGGS-C1V1	Section of Viral Vector Development, Center for Genetic Analysis of Behavior, National Institute for Physiological Sciences	N/A
AAV-DJ-CAGGS-coGHCR	Section of Viral Vector Development, Center for Genetic Analysis of Behavior, National Institute for Physiological Sciences	N/A
AAV-6-CAGGS-EGFP	Section of Viral Vector Development, Center for Genetic Analysis of Behavior, National Institute for Physiological Sciences	N/A
AAV-6-CAGGS-human rhodopsin	Section of Viral Vector Development, Center for Genetic Analysis of Behavior, National Institute for Physiological Sciences	N/A
AAV-6-CAGGS-ChrimsonR	Section of Viral Vector Development, Center for Genetic Analysis of Behavior, National Institute for Physiological Sciences	N/A
AAV-6-CAGGS-coGHCR	Section of Viral Vector Development, Center for Genetic Analysis of Behavior, National Institute for Physiological Sciences	N/A
Chemicals, peptides, and recombinant proteins		
Ames' medium	Merck	A1420
Mydrin-P (0.5% tropicamide and 0.5% phenylephrine)	Santen	N/A
Protease inhibitor cocktail	Merck	539131
Nitrocellulose membranes	Pierce Biotechnology, Inc.	24580
5% skim milk	Bio-Rad Laboratories, Inc.	190-12865
WB Stripping Solution	Nacalai Tesque	05364-55
4% paraformaldehyde (PFA)	Nacalai Tesque	11850-14
DAPI Fluoromount-G	SouthernBiotech	0100-20
All trans-retinal	Sigma-Aldrich	Cat#R2500
11-cis retinal	Toronto research chemicals	Cat#R239860
Critical commercial assays		
cAMP Gi kit	Cisbio	Cat #62AM9PEB
Situ Apoptosis Detection Kits	Chemicon International	Cat #S7165
Experimental models: Cell lines		
HEK 293T cells	ATCC	CRL-3216; RRID: CVCL_0063

(*Continued on next page*)

Continued

REAGENT or RESOURCE	SOURCE	IDENTIFIER
Experimental models: Organisms/strains		
Mouse: Pde6brdl (C3H/HeJJcl, rd1)	CLEA Japan	RRID: IMSR_JCL:MIN-0001
Mouse: C57BL/6JJcl	CLEA Japan	RRID: MGI:3055581
Mouse: RhoP23H/+ (B6.129S6(Cg)-Rhotm1.1Kpal/J, P23H)	Jackson Laboratory	017628; RRID: IMSR_JAX:017628
Software and algorithms		
MC Rack software (V 4.6.2)	Multi Channel Systems	N/A
Off-line Sorter software (version 4.4.0)	Plexon	N/A
NeuroExplorer 5 software (version 5.115)	Nex Technologies	N/A
ANY-maze tracking software	Stoelting	N/A
Move-tr/2D tracking software	Library	N/A
IBM SPSS Statistics 26	IBM	N/A
Other		
Active contact lens electrodes	Mayo	N/A
PuREC acquisition system	Mayo	N/A
Hemisphere LS-100 Stimulator	Mayo	N/A
HD Pro Webcam C920	Logitech,	N/A
B1-760HD	Acer Inc	N/A
Infinite M1000PRO	Tecan	N/A
JEM-1400Plus	JEOL	N/A
PVDF membrane	Merck	HVLP01300
LSM710	Carl Zeiss	N/A
DMEM	Nakarai	09891-25
Envisu R4310	Leica	N/A
Shimadzu LC20A	Shimadzu	N/A
Silica column (Ultrasphere 5um, SI 250 x 4.6mm	Avantor	Cat#235341

RESOURCE AVAILABILITY

Lead contact

Further information and requests for resources and reagents should be directed to and will be fulfilled by the lead contact, Toshihide Kurihara(kurihara@z8.keio.jp).

Materials availability

This study did not generate new unique reagents. All materials in this study will be made available on request to the lead contact. A material transfer agreement will be required prior to sharing of materials.

Data and code availability

The data that support the findings of this study are available from the lead contact upon request.

EXPERIMENTAL MODEL AND STUDY PARTICIPANT DETAILS

Study approval

All of the animal experiments were conducted in accordance with protocols approved by Institutional Animal Care and Use Committee of Keio University School of Medicine (#2808).

Mice homozygous for the retinal degeneration alleles *Pde6b*^{rdl} (C3H/HeJJcl, *rd1*) and WT C57BL/6J were obtained from CLEA Japan, Inc. Mice heterozygous for the retinal degeneration alleles *Rho*$^{P23H/+}$ (B6.129S6(Cg)-*Rho*$^{tm1.1Kpal}$/J, P23H) were obtained from Jackson Laboratory. Animals were maintained under 12-h light:12-h-dark conditions. For animals bred in house, littermates of the same sex (male) were

randomized to experimental groups. All of the animal experiments were conducted in accordance with protocols approved by Institutional Animal Care and Use Committee of Keio University School of Medicine.

METHOD DETAILS

Immunohistochemistry

The protocol for immunohistochemistry was previously described.[25] The retinas were incubated in PBS with 1% Triton X-100 and 0.5% Tween 20 for 1 h at room temperature and in 4% BSA for 1 h at room temperature and then incubated overnight at 4°C with primary antibodies: anti-FLAG (1:500, Merck, Darmstadt, Germany) and anti-PKCα (1:100, Abcam, Cambridge, UK) in blocking buffer. Secondary anti-rabbit, conjugated with Alexa TM488 or 594 (1:1000; Abcam), were applied for 1 h at room temperature.

Vector production and purification

GHCR construct were designed as previously reported[24]. GHCR, coGHCR, ChrimsonR, C1V1 amd human rhodopsin genes were cloned to pAAV-CAGGS-MCS. Type 2, 6, DJ serotypes of rAAV vectors were prepared using the AAV Helper Free Packaging System (Cell Biolabs, San Diego, CA, USA). The serotypes were produced in HEK 293T cells using a helper virus-free system and were purified using two $CsCl_2$ density gradients and titrated by quantitative polymerase chain reaction. Final preparations were dialyzed against phosphate-buffered saline (PBS) and stored at -80°C.

Virus injection

The mice were anesthetized with a combination of midazolam, medetomidine and butorphanol tartrate at doses of 4 mg/kg, 0.75 mg/kg and 5 mg/kg of body weight and placed on a heating pad that maintained their body temperatures at 35°C–36°C throughout the experiments. An aperture was made next to the limbus through the sclera with a 30-gauge disposable needle, and a 33-gauge unbeveled blunt-tip needle on a Hamilton syringe was introduced through the scleral opening into the vitreous space for intravitreal injections and introduced through the scleral opening along the scleral interior wall into the subretinal space for subretinal injections. Each eye received 1 μl in intravitreal or 0.4 μl in subretinal injection of vehicle (PBS) or vector at a titer of 1.0×10^{12} vg/ml (AAV-2 and AAV-DJ) or 1.0×10^{11} vg/ml (AAV-6).

Multielectrode array recordings

All of the procedures were performed under dim red light. The mice were anesthetized and euthanized by quick cervical dislocation. Following enucleation, the retina was dissected at room temperature in Ames' medium bubbled with 95% O2/5% CO2 (A 1420; Merck). The separated retina was placed on a cellulose membrane, and RGC was directed to the electrode and was gently contacted against MEA (MEA2100-Systems; Multi Channel Systems, Reutlingen, Germany) under suction pressure. During the experiment, the retinas were continuously perfused with Ames' medium bubbling at 34°C. at a rate of 1-2 ml/min. Recorded signals were collected, amplified, and digitized using MC Rack software (Multi Channel Systems). Retinas were perfused for 30 min in darkness before recording responses. 400, 470, 525, 570, 610, 630 and 660 LED was used in spectral sensitivity examination and white LED was used in the other experiment.

Uniform full-field light stimulation was presented for 1 seconds at 60-second intervals. Signals were filtered between 200 Hz (low cutoff) and 20 kHz (high cutoff). A threshold of 40 μV was used to detect action potentials, and action potentials from individual neurons were determined via a standard expectation–maximization algorithm using Off-line Sorter software (Plexon, Dallas, TX, USA). The results were plotted using NeuroExplorer software (Nex Technologies Colorado Springs, CO, USA).

ERG analyses

ERGs were recorded according to a previous report.[25] Animals were dark-adapted for 12 h and prepared under dim red illumination. The mice were anesthetized with a combination of midazolam, medetomidine and butorphanol tartrate at doses of 4 mg/kg, 0.75 mg/kg and 5 mg/kg of body weight, respectively and were placed on a heating pad that maintained their body temperature at 35°C–36°C throughout the experiments. The pupils were dilated with a mixed solution of 0.5% tropicamide and 0.5% phenylephrine (Mydrin-P; Santen, Osaka, Japan). The ground electrode was a subcutaneous needle in the tail, and the reference electrode was placed subcutaneously between the eyes. The active contact lens electrodes (Mayo, Inazawa, Japan) were placed on the corneas. Recordings were performed with a PuREC acquisition system (Mayo). Responses were filtered through a bandpass filter ranging from 0.3 to 500 Hz to yield a- and b-waves. White LED light stimulations of 10.0 log cd-s/m^2 were delivered via a Hemisphere LS-100 Stimulator (Mayo). The amplitudes were measured and analyzed based on ISCEV (International Society for Clinical Electrophysiology of Vision) standard. More specifically, rod response was obtained by a program with a dark-adapted 0.01 ERG (0.01 cds/m^2), mixed response by a dark-adapted 3.0 ERG (3.0 cds/m^2), and cone response by a light-adapted 3.0 ERG (3.0 cds/m^2 flash with 30 cd/m^2 for background).

VEP analyses

The measuring electrodes were placed more than one week before the measurement. The mice were anesthetized with a combination of midazolam, medetomidine and butorphanol tartrate at doses of 4 mg/kg, 0.75 mg/kg and 5 mg/kg of body weight, respectively. The animals were placed in a stereotaxic holder. A stainless-steel screw (M1.0×6.0 mm) inserted through the skull into the both visual cortex (1.5 mm laterally to the midline, 1.5 mm anterior to the lambda), penetrating the cortex to approximately 1 mm, served as a measuring electrode. Animals

were dark-adapted for 12 h and prepared under dim red illumination. At the time of the measurement, the mice were anesthetized again with the same doses. Visual stimuli were generated by a white LED flashes (3 cds/m^2). Signals were acquired and analyzed with a PuREC acquisition system (Mayo). Signals were low-pass filtered at 300 Hz and averaged over the 60 trials.

LDT recording

Mice were tested in a 30 × 45 × 30-cm box, containing equally sized light and dark chambers connected by a 5 × 5-cm opening via which mice could move freely. The bright half of the box was illuminated from above by a white LED. The illumination intensity of measured at the floor level. The animals were placed in the bright half and movement recorded (HD Pro Webcam C920, Logitech, Lausanne, Switzerland). A trial lasted 10 min, and then the testing apparatus was dismantled and cleaned with 70% ethanol. Videos were analyzed using ANY-maze tracking software and were validated by comparison with manual analysis. Time spent in the bright half was recorded.

VRT recording

Mice were tested in a 216 × 148 × 220-mm box, containing equally sized light and dark chambers connected by a 120 × 60-mm opening via which mice could move freely. The size of the tablet was 107 × 9.9 × 193-mm (B1-760HD, Acer Inc, New Taipei, Taiwan). The resolution of the display was 1280 × 720 pixels, and the resolution of the videos was 640 × 480 pixels. The luminance of all videos was 20 $\pm$ 3 lux. All videos were presented without sound. The box was illuminated from above by a white LED with 10 lux. The illumination intensity of measured at the floor level. The animals were placed in the bright half and movement recorded (HD Pro Webcam C920, Logitech, Lausanne, Switzerland). A trial lasted 15 min, and then the testing apparatus was dismantled and cleaned with 70% ethanol. Videos were analyzed using Move-tr/2D tracking software (Library, Tokyo, Japan) and were validated by comparison with manual analysis. Time spent in the bright half was recorded.

Gi/o coupled GPCR activation assay

HTRF-based cAMP detections were conducted with cAMP Gi kit (Cisbio #62AM9PEB, Bedford, MA) according to the manufacturer's instructions. HEK293T cells were kept in DMEM (12-well plate) supplemented with 10% (v/v) fetal bovine serum in a humidified incubator at 37°C 5% CO2. HEK293T cells were seeded on a 12-well plate at 1x10^5 cells/well, and on the day 2, 1x10^6 vg/well/500 µl of AAV vector (AAV-DJ-GAGGS, AAV-DJ-CAGGS-GHCR, AAV-DJ-CAGGS-coGHCR) was added and transfected. Transfected cells were kept in the dark for 2 days. On the day 4, after seeding in a 384-well plate at 6,500 cells/well/5 ul and incubating for 4 hours in the dark. Photo-stimulation (525 nm LED 10^{16} photons/cm^2/s 1 minute) was performed. The signal was detected using plate reader Infinite M1000PRO (Tecan, Männedorf, Switzerland).

TEM

Eye cups were fixed with aldehyde/DMSO at 37°C for 2–4 h and then eye cups were cut in half on their dorsal-ventral axis and fixed again for several minutes. Ultrathin sections were cut with a diamond knife. Specimens were examined using a transmission electron microscope (JEM-1400Plus).

Preparation of cryosections of retinas

Enucleated eyes were fixed for 20 min in 4% paraformaldehyde (PFA) in PBS and then dissected as previously described.[61] The obtained tissues were post-fixed overnight in 4% PFA in PBS and stored in methanol at –20°C. Cryosections of retinas (12 µm) were prepared as previously described,[62] after the eyeballs were immersed overnight in 4% PFA. The retinal sections were observed using a confocal microscope (LSM710; Carl Zeiss, Jena, Germany).

TUNEL assay

After the cryosection mentioned above, cell apoptosis was detected by TUNEL using ApopTag *In Situ* Apoptosis Detection Kits (Chemicon International, Darmstadt, Germany; cat. #S7165) according to the manufacturer's instructions. Nuclei were counterstained with DAPI. The retinal sections were observed using a confocal microscope (LSM710; Carl Zeiss, Jena, Germany).

OCT imaging

The thickness of the retina was analyzed by an SD-OCT system (Envisu R4310; Leica, Wetzlar, Germany) tuned for mice. The imaging protocol entailed a 3 mm×3 mm perimeter square scan sequence producing a single en-face image of the retina through a 50-degrees field of view from the mouse lens, following mydriasis. The en-face image consisted of 100 B-scan tomograms with each B-scan consisting of 1000 A-scans. The retinal thickness of 150 µm from the optic disc of each quadrant was measured.

HPLC analysis of retinal

After 15 hours of dark adaptation, mice were exposed to light adaptation at 1000 lux for 10 minutes. The mice were subsequently sacrificed, and the removed mouse retinas were homogenized. Hydroxylamine was added to the homogenized retinas for oximation. The retinal-oximes

was dissolved in hexane to make a sample for HPLC analysis. All of these processes were performed under dim red lights. Two retinas were used per assay.

Retinal oximes were analyzed by HPLC (Shimadzu LC20A series, Japan) with a silica column (Ultrasphere 5um, SI 250 x 4.6mm, Avantor, USA). The mobile phase consisted 96.0%(v/v) hexane, 4.0%(v/v) ethyl acetate and the flow rate was 1.0mL/min. The column temperature was 35°C. Absorbance at 360 nm was monitored for retinal oximes. Each retinal isomer was quantified from the area of the corresponding peak based on a calibration retinal standard reagent. All trans-retinal (Sigma-Aldrich) and 11-cis retinal (Toronto research chemicals) were used as standard reagents.

Data and software availability

Raw MEA spike data were sorted offline to identify single units using Offline Sorter software (version 4.4.0) (Plexon). Spike-sorted data were analyzed with NeuroExplorer 5 software (version 5.115) (Nex Technologies). The data that support the findings of this study are available from the corresponding author on request.

QUANTIFICATION AND STATISTICAL ANALYSIS

All of the results are expressed as the mean ± SEM. The averaged variables were compared using the unpaired t-test and the one-way ANOVA test. Tukey's test was used for multiple comparisons. P-values of less than 0.05 were considered statistically significant. All experiments were randomized. SPSS 26 (IBM Corporation, Armonk, NY) was used for statistical analysis.